hydrogen

MDPI

Supplementary Materials

Simulation of Biogas Conversion Using Porous Solid Oxide Electrochemical Cells: Virtual Prototyping

Konakpo Parfait Kamara [1,2] Gérard Merlin [3], Gaoussou Bamba [2], Florence Druart [1] and Jonathan Deseure [1,*]

Nomenclature

a_v	specific surface area $m^2.m^{-3}$
d_i	characteristic diameter of the molecule in Angström
i	total current density of the cell, $A.m^{-2}$
d_g	grain diameter, m
d_{pores}	pores diameter, m
i_a	anodic current transfer the points of triple contact, $A.m^{-3}$
$i_{a,0}$	Exchange current density at the interface of the anode, $A.m^{-2}$
k	Boltzmann constant en m^2 kg s^{-2} K^{-1}
k_2	Coefficient of backward the steam reforming kinetic, $mol.g_{cat}^{-1}.Pa^{-4}.s^{-1}$
k_3	Coefficient of dry reforming, $mol.g_{cat}^{-1}.s^{-1}$
k_4	Coefficient of forward kinetic of water gas shift reaction, $mol.g_{cat}^{-1}.Pa^{-2}.s^{-1}$
k_5	Coefficient of backward kinetic of water gas shift reaction, $mol.g_{cat}^{-1}.Pa^{-4}.s^{-1}$
k_d	Coefficient de Fuller, Schtteler and Gidding [18]
$p_{réf}$	Atmospheric pressure Pa
p_i	Partial pressure species *i*, Pa
p_m	Partial pressure of the mixture Pa
dr	Kinetic of dry reforming, $mol.m^{-3}.s^{-1}$
rgs	Kinetic of water shift gas, $mol.m^{-3}.s^{-1}$
rvr	Kinetic of steam reforming, $mol.m^{-3}.s^{-1}$
u	Rate m/s
v_1	Steam reforming reaction kinetic data on the basis of the catalyst mass, $mol.g_{cat}^{-1}.s^{-1}$
v_2	Dry reforming reaction kinetic data on the basis of the catalyst mass, $mol.g_{cat}^{-1}.s^{-1}$
w_i	Mass fraction of species, *i*

x_i	Molar fraction of species, *i*
C_{p_i}	Molar heat capacity of the species at constant pressure, J.mol^{-1}.K^{-1}
D_{ik}	Binary Coefficient diffusion, $m^{-2}.s^{-1}$
$D_{ik,eff}$	Effective binary diffusion coefficient, $m^{-2}.s^{-1}$s
$E_{a\ ou\ c,0}$	Equilibrium potential of the electrode, V en W/m^3
E_{dr}	Heat generated from dry reforming, W/m^3
E_{gs}	Heat generated from water gas shift, W/m^3
E_{vr}	Heat generated from steam reforming, W/m^3
$E_{irr,a}$	Heat generated from anodic over voltage, W/m^3
$E_{irr,c}$	Heat generated from cathodic over voltage, W/m^2
E_{rev}	Heat generated from electrochemical reaction, W/m^3
$E_{ohm,ion}$	Heat generated from Joule Effect of YSZ, W/m^3
$E_{ohm,élec}$	Heat generated from Joule Effect of electrodes, W/m^3
K_{CO_2}	Adsorption coefficient of CO_2, Pa^{-1}
K_{CH_4}	Adsorption coefficient of CH_4, Pa^{-1}`
J_i	Molar flux density *i,* kg.m^2.s^{-1}
M_i	Molecular weight of the species *I,* g/mol
N_i	Molar flow density of the species i, mol.s^{-1}.m^{-2}
$Q_{\ j}$	Current sources, A.m^{-3} ou A.m^{-2}
Q_c	Heat sources, W/m^3
$S_{g_{Lenhert}}$	Reactive surface of Lenhert *et al.*, m^2/g_{cat}
$S_{g_{Ri}}$	Reactive surface of Richardson *et al.*, m^2/g_{cat}
$\left(\frac{S_s}{V}\right)$	Specific surface, m².m^{-3}
T*	Dimensionless Variable of Temperature
V_{ion}	Ionic potential, V
$V_{élec}$	Electronic potential, V
$\alpha_{a\ ou\ c}$	Symmetry factor
γ_c	Pre-exponential corrective Coefficient, $A.m^{-2}$
ε	Porosity %
η_{aouc}	Anodic or cathodic overvoltage, V

κ	Permeability coefficient, m²
λ	Thermal conductivity, mW.m^{-1}.K^{-1}
μ	Dynamic viscosity, Pa.s
μ_{mix}	Dynamic viscosity of the gas mixture of simple method Herming & Zipperer Pa.s
ρ	Density, kg.m^{-3}
σ_{ion}^{eff}	Effective ionical conductivity, Sm^{-1}
σ_{ion}	Ionic conductivity, Sm^{-1}
τ	Tortuosity
τ_c	Shear stress, (N/m²)
ϕ	Heat flow, W.m^{-2}
$\varphi_{NI,YSZ}$	Volume fraction Ni, or YSZ %
χ	Characteristic energy the molecule, J
$\Delta_r H_T^\circ$	Reaction enthalpy at temperature T, J/mol
ΔC	Concentration gradient, mol.m^{-3}
ΔT	Temperature gradient, °C or K
Ω_i	Integral case of collision *i*

I. Expression of reaction rate kinetic

Two internal reforming reactions are catalyzed at the surface of nickel cermet component. The high temperature operation improves solid oxide electrochemical cell (SOEC) catalysis reforming reactions and thus allows a power supply to the anode hydrocarbonS From Lehnert *et al.* [18] study, it is possible to determine the expression of the kinetic reaction of steam reforming by ratio of catalyst compound (mol.g$_{cat}^{-1}$.s^{-1}), is written as follow:

$$v_1 = k_1 exp\left(-\frac{27063}{T}\right) P_{CH_4} P_{H_2O} - k_2 exp\left(-\frac{233}{T}\right) P_{CO} {P_{H_2}}^3 \quad \text{(S1)}$$

However, Lehnert *et al.* [14] showed a surface corrected calculated $S_{g_{Lenhert}}$ (m²/g$_{cat}$) using the surface area of the porous material $\left(\frac{S_s}{V}\right)_{cat}$(m²/m³), a new expression of the kinetics of steam reforming rvr expressed in mol/(m³.s¹):

$$rvr = \frac{v_1}{S_{g_{Lenhert}}} \left(\frac{S_s}{V}\right)_{cat} \quad \text{(S2)}$$

Similarly, the dry reforming reaction kinetics is expressed from the work of Richardson *et al.* [19] as follow:

$$v_2 = k_3 \frac{K_{CO_2} K_{CH4} P_{CO_2} P_{CH4}}{\left(1 + K_{CO_2} P_{CO_2} + K_{CH4} P_{CH4}\right)^2} \quad \text{(S3)}$$

While v_2 is the reaction kinetics (in mol.g$_{cat}^{-1}$.s^{-1})), k_3 the kinetic constant (in mol.g$_{cat}^{-1}$.s^{-1}), K constant for the equilibrium of adsorption (in Pa^{-1}) and Pi partial pressures (in Pa).

This phrase is adapted to our material by taking the value of specific surface reaction of the author's material $S_{g_{Ri}}$(en m^2/g_{cat}) [19] in $mol/(m^3.s^1)$:

$$rdr = \frac{v_2}{S_{g_{Ri}}}\left(\frac{S_s}{V}\right)_{cat} \quad (S4)$$

Finally, the kinetics of water gas shift takes place throughout the anode volume. Therefore, there would be no need for correction. It is also obtained from the work of Lenhert *et al.* [18] $mol.m^{-3}.s^{-1}$:

$$rgs = k_4 P_{CO} P_{H_2O} - k_5 P_{CO_2} P_{H_2} \quad (S5)$$

II. Charge balance

The electrical current continuity equation has been solved to obtain the current density distribution. Since there are no sources of current density in cathode and interconnect, the solved equation is expressed as follows:

$$i = \sigma.E \quad (S6)$$

Where i is the current density, σ is the ionic or electronic conductivity and E is the electric field. The current density source at cathode/electrolyte interface is ruled by a Butler-Volmer law.

In steady state, the equation solved by the software is:

$$\nabla.i = 0 \quad (S7)$$

The continuity equation should be taken into account in the porous media YSZ as follow:

$$\nabla.i = \nabla\left(\sigma_{ion}^{eff} V\right) \quad (S8)$$

With the evolution of ionic conductivity as function of temperature [20]:

$$\sigma_{YSZ} = 0{,}33410^5 exp\left(-\frac{10300}{T}\right) \quad (S9)$$

Using the correction of porous media:

$$\sigma_{ion}^{eff} = \sigma_{YSZ}\frac{(1-\varepsilon)}{\tau} \quad (S10)$$

In order to solve the equation (S8) boundary conditions is required. Hydrogen is consumed by an electrochemical reaction at anode/electrolyte interface. For high hydrogen concentration, the electrochemical reaction is enhanced. Therefore j_r is the current conditions at anode /cathode and the general form of this law is given by the expression below [21]

$$i_a = j_0\left[\exp\left(\frac{-\alpha_r nF\eta}{RgT}\right) - \exp\left(\frac{\alpha_o nF\eta}{RgT}\right)\right] \quad (S11)$$

The electric potential imposed on the interface of channel/cathode is Vion
All other walls are considered insulated
In the present model, anode overpotential will be fixed by the following expression:

$$\eta = E^{\,input} - E^{\,OCV} \quad (S12)$$

Where E^{input} is the imposed artificial potential and E^{OCV} is the equilibrium voltage.

III. Main parameter values

a. Geometric parameters

As mentioned, the cells were involved porous materialS The effect of variation of the porosity and permeability used in the calculations will be very low. The microstructure was fixed during manufacturing conditionS Knowing the grain size while measuring the porosity ε, it will be possible to determine the specific surface area " a_v " ($m^2.m^{-3}$) and the pore diameter " d_{pores}" of the composite medium through these equations:

$$a_v = \frac{6}{d_g(1-\varepsilon)} \quad \text{(S13)}$$

$$d_{pores} = \frac{2}{3}\frac{\varepsilon}{(1-\varepsilon)}d_g \quad \text{(S14)}$$

By introducing the tortuosity τ that takes into account the actual path of the gas in porous media, it is possible to determine the coefficient of permeability κ (in m^2) of the material. It characterizes the ability of the medium passing a fluid through its pores (Darcy's law) and is expressed according to the Kozeny-Carman relation such as:

$$\kappa = \frac{\varepsilon^3 {d_g}^2}{72\tau(1-\varepsilon)^2} \quad \text{(S15)}$$

At the anode, the methane reforming reactions are catalyzed in the nickel grain surface. It was necessary to define the specific surface area $\left(\frac{S_s}{V}\right)$ expressed in $m^2.m^{-3}$ which takes into account the composition of the material, that is to say the volume fraction φ_{Ni} and the surface area developed by the catalyst:

$$\left(\frac{S_s}{V}\right) = \varphi_{Ni}.\, a_v \quad \text{(S16)}$$

Thus, the parameters used to define the microstructure in the numerical model are presented in Table S1 below:

Table S1. Intrinsic parameters of materials microstructure.

Parameters	Values
Catalyst layer	
Grains size, d_g (m)	1e-6
Porosity, ε (%)	0,4
Ni volume fraction in the electrode, ϕ_{Ni}	0,5
Tortuosity of gas, τ	4
Specific surface of cermet, a_v ($m^2.m^{-3}$)	computed
Specific surface of nickel catalyst, $(S_s/V)_{cat}$($m^2.m^{-3}$)	computed
Permeability, κ (m^2)	computed

b. Mass balance parameters

According to ideal gas law:

$$PV = nRT \quad \text{(S17)}$$

The composition of the mixture is defined by the mole fraction expressed as follow:

$$x_i = \frac{n_i}{n_{tot}} \quad et \quad \sum x_i = 1 \quad \text{(S18)}$$

Where: $\boldsymbol{n_i}$ is the number of moles of component i in the mixture $\boldsymbol{n_{tot}}$ is the total number of moles of the mixture equal to the sum of $\boldsymbol{n_i}$. The total pressure of the mixture pm is the sum of the partial pressure pi (Pa) of the gas, it is written as follow:

$$p_m = \sum_{,} p_i \qquad et \qquad p_i = \sum_{,} x_i . p_{atm} \tag{S19}$$

The values of coefficients used in the model and their references are given in Table S2 below and x_k is the mole fraction of species k calculated at all pointS It can be written as:

$$x_k = \frac{w_k}{M_k} M_m \tag{S20}$$

M_m is the molar mass of the gas mixture. It takes into account the mass proportion and the molecular weight of each species:

$$M_m = \left(\sum_i \frac{w_i}{M_i} \right)^{-1} \tag{S21}$$

Table S2. Values of kinetic parameters of reactions

Parameters	Values	Ref.
Steam Reforming		
Forward kinetic Coefficient, $k_1\ (mol.g_{cat}^{-1}.Pa^{-2}.s^{-1})$	4,69e-4	[18]
Backward kinetic Coefficient, $k_2\ (mol.g_{cat}^{-1}.Pa^{-4}.s^{-1})$	3,91e-27	[18]
Reactive surface, $S_{g_{Lenhert}}(m^2/g_{cat})$	8,6e-2	[18]
Specific surface area $(S_s/V)_{cat}\ (m^2/m^3)$	computed	Eq. A14
Dry reforming		
Forward kinetic Coefficient, $k_3\ (mol.g_{cat}^{-1}.s^{-1})$	1290 exp(-12276/T)	[19]
Equilibrium adsorption coefficient CO_2, $K_{CO_2}(Pa^{-1})$	2,5765e-7 exp(4527/T)	[19]
Equilibrium adsorption coefficient CH_4, $K_{CH_4}(Pa^{-1})$	2,5667e-7 exp(4893/T)	[19]
Reactive surface $S_{g_{Ri}}(m^2/g_{cat})$	8.6e-2	[19]
Specific surface area, $(S_s/V)_{cat}\ (m^2/m^3)$	computed	Eq. A14
Water shift gas		
Forward kinetic Coefficient, $k_4\ (mol.g_{cat}^{-1}.Pa^{-2}.s^{-1})$	1,73e-2	[18]
Backward kinetic Coefficient, $k_5\ (mol.g_{cat}^{-1}.Pa^{-4}.s^{-1})$	0,98	[18]
Hydrogen oxydation		
Symmetry factor, α_a	0,5	[21]
Potential electrode balance, $E_{a,0}(V)$	0	[21]
Exchange current density, $i_{a,0}\ (A.m^{-2})$	1e12	[21]

The transport property is defined by a gradient law, Poisson's equation. In the case of dynamic viscosity, the flow momentum created by the velocity gradient imposed on the fluid results in the shear stress τ_c (N/m²):

$$\tau_c = \mu \frac{du}{dv} \quad \text{(S22)}$$

To calculate the dynamic viscosity of the mixture, it is necessary to express the μ_i dynamic viscosity of each species defined by the kinetic theory of gases [22]:

$$\mu_i = 2{,}669310^{-6} \frac{\sqrt{M_i T}}{d_i^2 \Omega_i} \quad \text{(S23)}$$

with Mi is the molar mass of the species i, di the characteristic diameter of the molecule (Angström) and Ωi the collision integral expressed through the empirical relations:

$$\Omega_i = \frac{1{,}16145}{(T^*)^{0{,}14874}} + \frac{0.52487}{\exp(0{,}77320T^*)} + \frac{2{,}16178}{exp\,(2{,}43787T^*)} \quad \text{(S24)}$$

where T^* is the dimensionless temperature variable defined for the molecule as:

$$T^* = \frac{T}{(\chi/_k)} \quad \text{(S25)}$$

χ represents the characteristic energy of the molecule and k the Boltzmann constant. The values of (χ/k) expressed in Kelvin, are classified for each molecule in the Tables of Lennard-Jones [23]. To simplify the evaluation, only two major species of the gas mixture in each channel was considered, CH_4 / CO_2 (cf. TABLE S3).

Table S3. Viscosity parameters

Species	***Mi (g/mol)***	***di (***Å)	$(\chi/_k)$ **(K)**
CH_4	16	3 ,758	148,6
CO_2	44	3 ,941	195,2

μ the dynamic viscosity (Pa.s) depends on the composition of the gas mixture. Reid *et al.* [23] described the behavior of mixtures of fluids including gas, thus it is possible to use the simple method of Herming & Zipperer which is defined as follows:

$$\mu_{mix} = \frac{\sum(\mu_i x_i \sqrt{M_i})}{\sum(x_i \sqrt{M_i})} \quad \text{(S26)}$$

This method is a simplification of the method of Wilke's and allows to obtain reliable values of viscosity for mixtures which are not rich in hydrogen, errors for a hydrocarbon mixture ranging from 1.5 to 5%. In this case, the proportion of hydrogen in the same cell output remains low. However, another method should be used to express the viscosity if the amount of hydrogen reformed becomes consistent. On the other hand, in porous media, typically at electrode and electrolyte, Navier-Stokes equation is solved to describe the fluid distribution:

$$-\nabla.\left[\frac{\mu}{\varepsilon}(\nabla u + (\nabla u)^T)\right] + \nabla p + \frac{2\mu}{3\varepsilon}\nabla^2 u + \frac{\mu}{\kappa}u = 0 \quad \text{(S27)}$$

The microstructure of the pourous media was considered with ε the porosity and κ (m^2) the permeability of the material.

The binary diffusion coefficient of the gas depends on the temperature. It is calculated from the expression of Bird *et al.* [22], commonly used in the literature and defined as:

$$D_{ik} = \frac{k_d T^{1,75}}{p_{réf}(v_i^{1/3} + v_k^{1/3})^2}\sqrt{\frac{1}{M_i} + \frac{1}{M_K}} \quad \text{(S28)}$$

While vi and vk represent respectively the diffusion' molar volume of species $i\ an$, and the coefficient of kd Fuller, Schettler, and Giddings [24]. $M_i\ and\ Mk$ are the molecular weights of the species i and k in kg/mol, T is the temperature in K, $pref$ is the reference pressure given in Pa. The coefficiens are gathered in the Table S4

Table S4. Diffusion parameters

k_d	v_{N_2}	v_{O_2}	v_{H_2O}	v_{H_2}	v_{CH_4}	v_{CO_2}	v_{CO}
3,16e-8	17,9e-6	16,6e-6	12,7e-6	7,07e-6	30e-6	26,9e-6	18,9e-6

According to Bird *et al.* [22] the Bruggeman's expression is used in pours media, as follow:

$$D_{ik,eff} = D_{ik}\varepsilon^{\tau} \quad \text{(S29)}$$

Matrix diffusivity of, Stefan-Maxwell model is defined as follow, with a gas mixture, the influence of binary diffusivities of each species over others on diffusion flux of each species J_i such as:

$$J_i = \rho w_i \sum_k D_{ik} d_k \quad \text{(S30)}$$

For this, the matrix model Stefan-Maxwell in implemented in Comsol® Multiphysics, as follow:

Table S5. Stefan-Maxwell matrix.

Maxwell-Stefan diffusivity matrix:

D_{ik}

1	D_H2_H2O	D_CH4_H2	D_H2_CO2	D_H2_CO	D_H2_N2	
D_H2_H2O	1	D_CH4_H2O	D_H2O_CO2	D_H2O_CO	D_H2O_N2	
D_CH4_H2	D_CH4_H2O	1	D_CH4_CO2	D_CH4_CO	D_CH4_N2	
D_H2_CO2	D_H2O_CO2	D_CH4_CO2	1	D_CO_CO2	D_CO2_N2	
D_H2_CO	D_H2O_CO	D_CH4_CO	D_CO_CO2	1	D_CO_N2	
D_H2_N2	D_H2O_N2	D_CH4_N2	D_CO2_N2	D_CO_N2	1	

m^2/s

c. Heat balance parameters

The expression of thermal conductivity ($W.m^{-1}.K^{-1}$) depends on the media:

In solid media, the conductivities will be constant in the range of simulated temperatures

In porous media, the effective conductivity λeff is an interaction that combines gas conduction λg through the pores with the solid material conduction λs in the following way:

$$\lambda_{eff} = \varepsilon\lambda_g + (1-\varepsilon)\lambda_s \quad \text{(S31)}$$

In a gaseous medium, they vary depending on the mixture composition and temperature. The conductivity of gas mixtures λg obeys complex lawS In first approximation, it is possible to use the formula (deviation ≈ 3%):

$$\lambda_g = \frac{\sum x_i \lambda_i M_i^{1/3}}{\sum x_i M_i^{1/3}} \quad \text{(S32)}$$

This expression reflects the composition of the gas with xi and Mi respectively the mole fraction and molar mass of species i; and the conductivity of each λi specieS The thermal conductivity of the gas in the vicinity of atmospheric pressure increases with temperature. At low pressures, between 0.01 and 1 MPa, the thermal conductivity increases, generally less than 10%.

Table S6. Expression of thermal conductivity of species according to the temperature [25].

Thermal Conductivity ($Mw.m^{-1}.K^{-1}$)	Expression
CH_4, λ_{CH_4}	$5{,}7381 + 0{,}04019\,T + 2{,}0627.10^{-4}T^2 - 8{,}3451.10^{-8}T^3$
CO_2, λ_{CO_2}	$-0{,}341914 + 0{,}0314\,T + 1{,}170458.10^{-4}T^2 - 1{,}281.10^{-7}T^3 + 5{,}7923.10^{-11}T^4 - 9{,}72044.10^{-15}T^5$
CO, λ_{CO}	$-0{,}42832 + 0{,}09941\,T - 5{,}96573.10^{-5}T^2 + 3{,}81583.10^{-8}T^3 - 1{,}43131.10^{-11}T^4 + 2{,}56748.10^{-15}T^5$
H_2, λ_{H_2}	$1{,}02672 + 0{,}74409\,T - 4{,}547.10^{-4}T^2 - 3{,}70833.10^{-9}T^3 + 2{,}67329.10^{-10}T^4 - 1{,}06021.10^{-13}T^5$
H_2O, λ_{H_2O}	$0{,}53 + 0{,}047093\,T + 4{,}9551.10^{-5}T^2$
N_2, λ_{N_2}	$-0{,}3721 + 0{,}10977\,T - 9{,}42549.10^{-5}T^2 + 8{,}05548.10^{-8}T^3 - 3{,}35367.10^{-11}T^4 + 5{,}15605.10^{-15}T^5$
O_2, λ_{O_2}	$-1{,}7536 + 0{,}1224\,T - 1{,}322444.10^{-4}T^2 + 1{,}7804.10^{-7}T^3 - 1{,}200176.10^{-10}T^4 + 2{,}9817302.10^{-14}T^5$

The molar heat capacity at constant pressure Cp_i of species i varies as a function of temperature. This Values are gathered in Table S7.

Table S7. Thermal capacity of endangered gas phase according to the temperature.

Thermal Capacity ($J.mol^{-1}.K^{-1}$)	Expression
CH_4, $C_{p_{CH_4}}$	$14{,}15 + 75{,}5.10^{-3}T - 17{,}99.10^{-6}T^2$
CO_2, $C_{p_{CO_2}}$	$45{,}35 + 8{,}688.10^{-3}T - 9{,}62.10^{-6}T^2$
CO, $C_{p_{CO}}$	$28{,}068 + 4{,}631.10^{-3}T - 0{,}258.10^{-6}T^2$
H_2, $C_{p_{H_2}}$	$27{,}01 + 3{,}509.10^{-3}T + 0{,}690.10^{-6}T^2$
H_2O, $C_{p_{H_2O}}$	$28{,}85 + 12{,}055.10^{-3}T + 1{,}006.10^{-6}T^2$
N_2, $C_{p_{N_2}}$	$27{,}27 + 4{,}93.10^{-3}T + 0{,}33256.10^{-6}T^2$
O_2, $C_{p_{O_2}}$	$30{,}255 + 4{,}207.10^{-3}T - 17{,}9910^{-6}T^2$

I. Geometry of the device

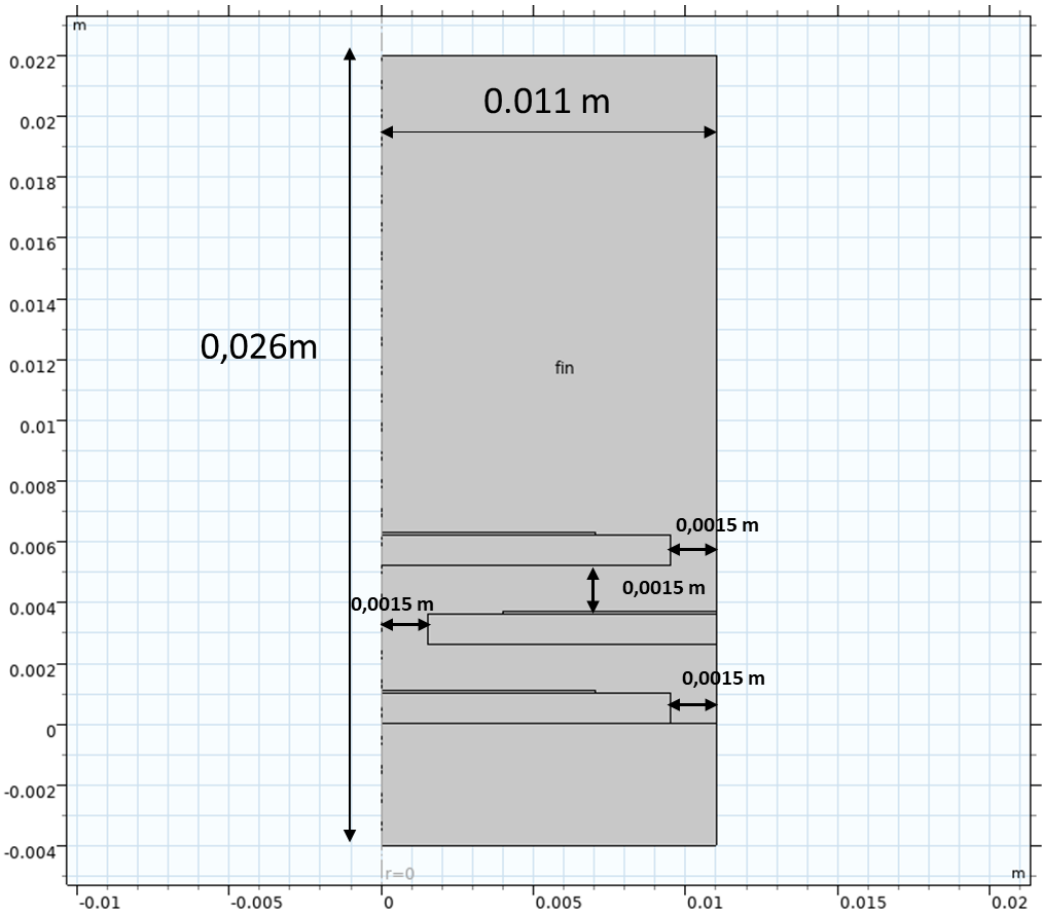

Figure S1. Geommetry of simulated cells

IV. Meshing sensitivity study

Table S8. Nodes and statistics of meshed domain: mesh boundaries layers (triangles).

Number of elements	Minimum element quality	Average element quality	Element area ratio	Mesh area (m^2)
3820	0.1372	0.786	7.911E -4	2.86 E -4

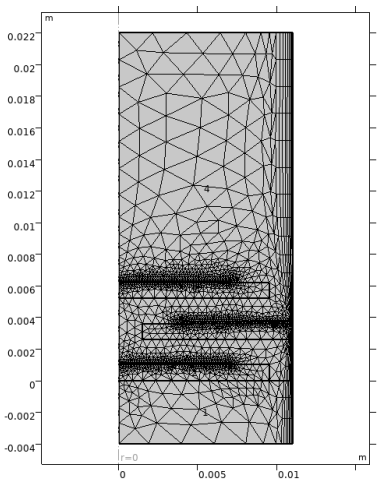

Figure S2. Boundary layers mesh**.**

Table S9. Nodes and statistics of meshed domain: mesh Free quad.

Number of elements	Minimum element quality	Average element quality	Element area ratio	Mesh area (m^2)
2070	0.3627	0.7878	8.82E -4	2.86 E -4

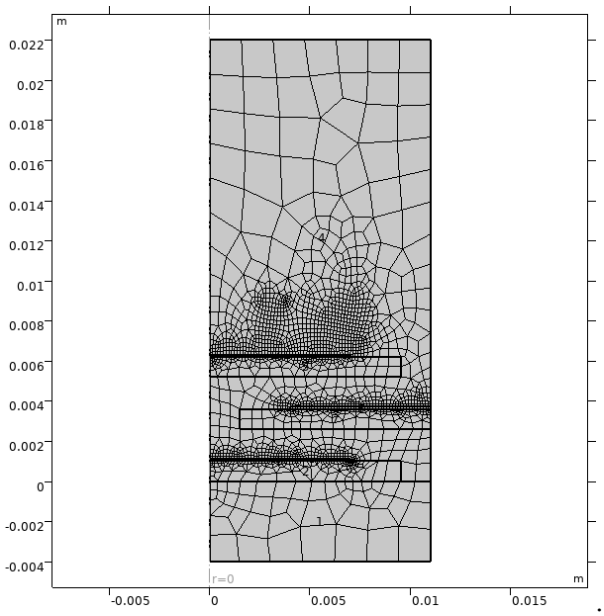

Figure S3. Free quad mesh.

For these both meshes the computing time is shorter than the triangular but with also less number of elementS We are less accurate for these meshes (Boundary Layers and Free Quad) and when compare methane partial pression for the triangular mesh with Boundary Layers and Free Quad meshes, the result is a bit better within the first configuration mesh (triangular).

Comparison of methane and hydrogen partials pression according to the type of mesh use.

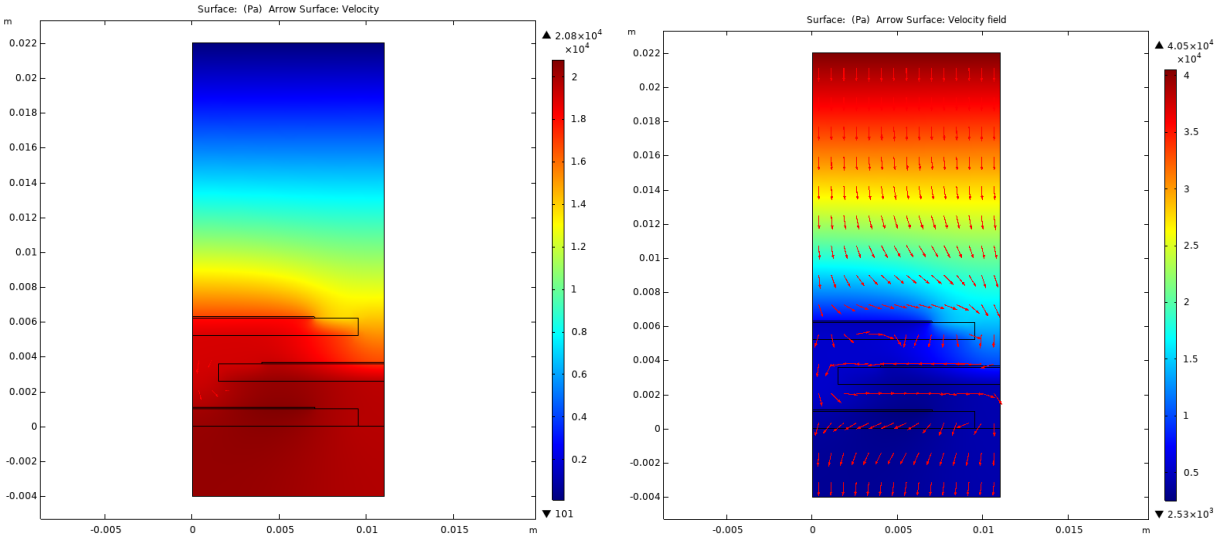

Figure S4. Hydrogen partial pression obtained using boundary layers mesh (left) using Free Quad mesh (right).

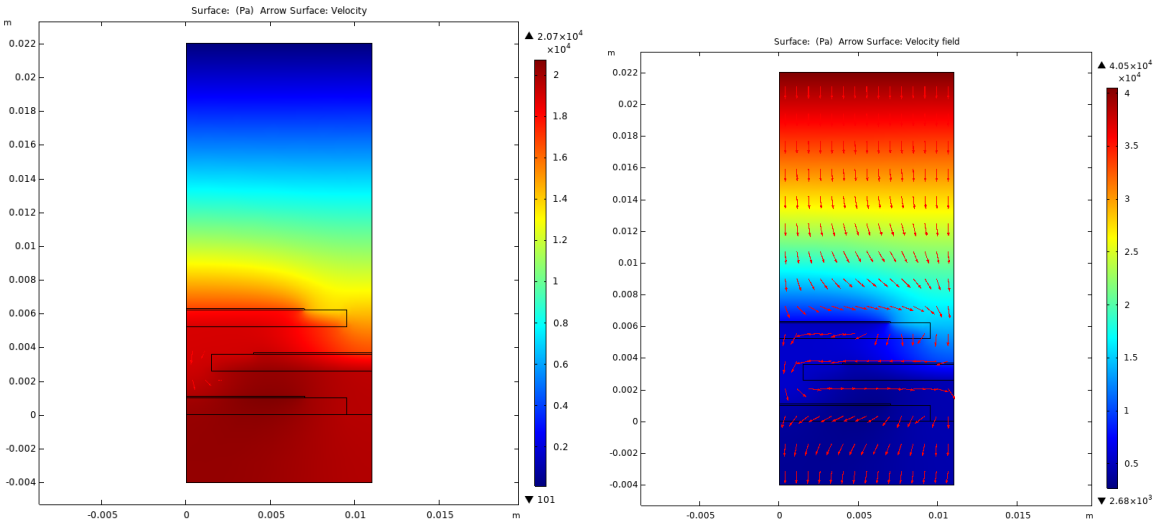

Figure S5. Methane partial pression obtained using boundary layers mesh(left) Methane partial pression obtained using Free quad mesh (right).

We can notice that the hydrogen production is not the same according to the mesh use. That's the same behavior for methane consumption.

II. Additional results

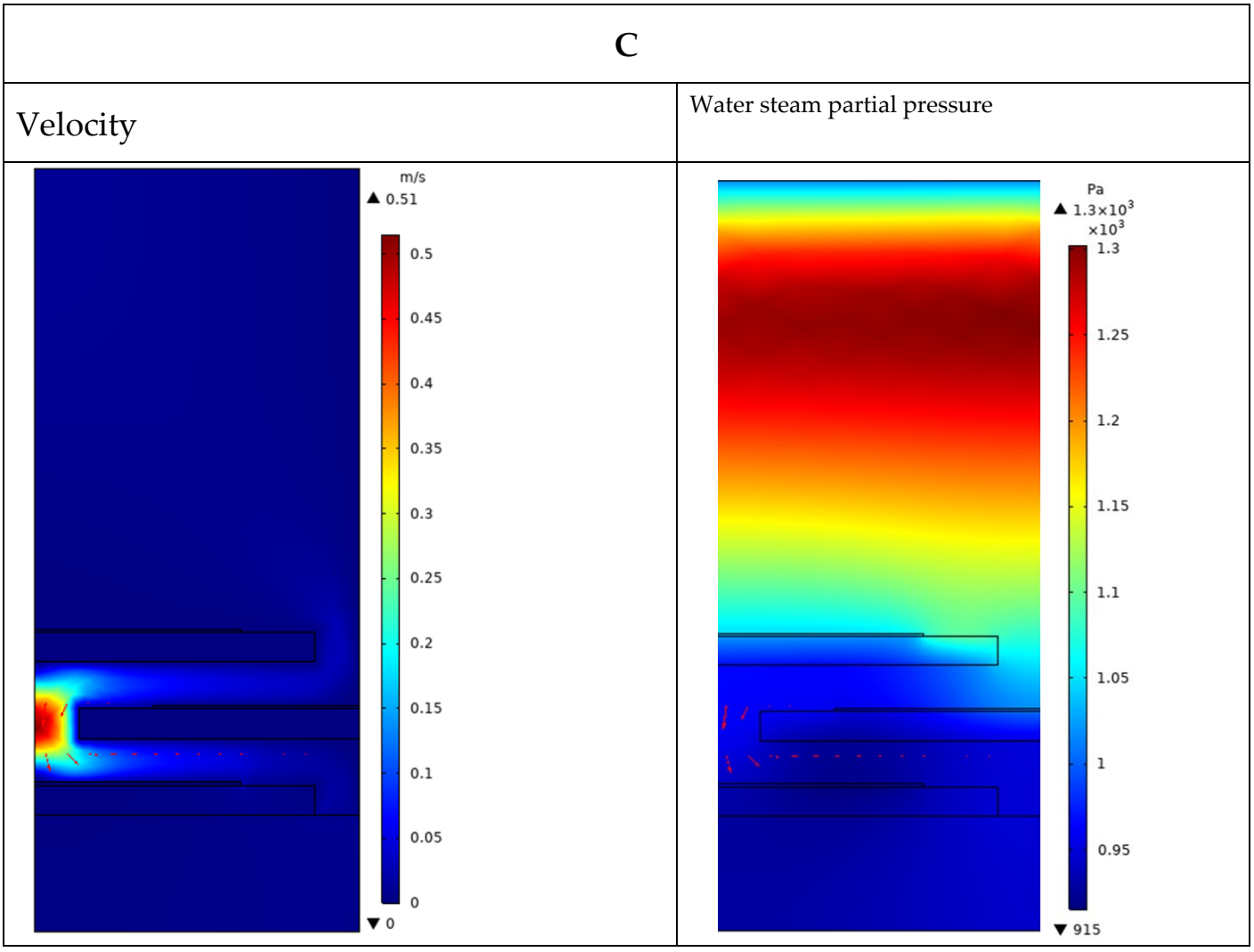

Figure S6. Velocity, partial pressure of steam for C case.

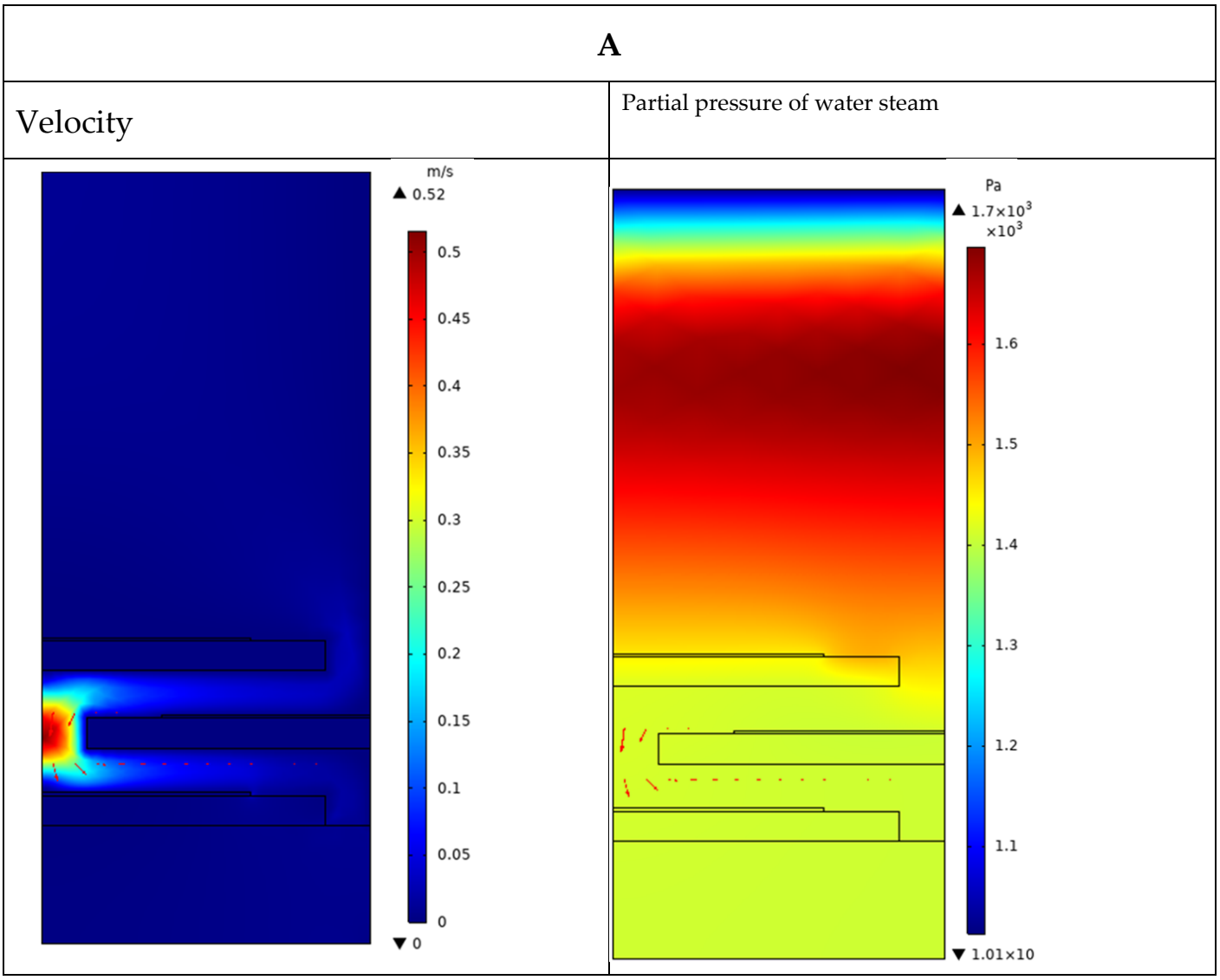

Figure S7. Velocity, partial pressure of steam for C case.

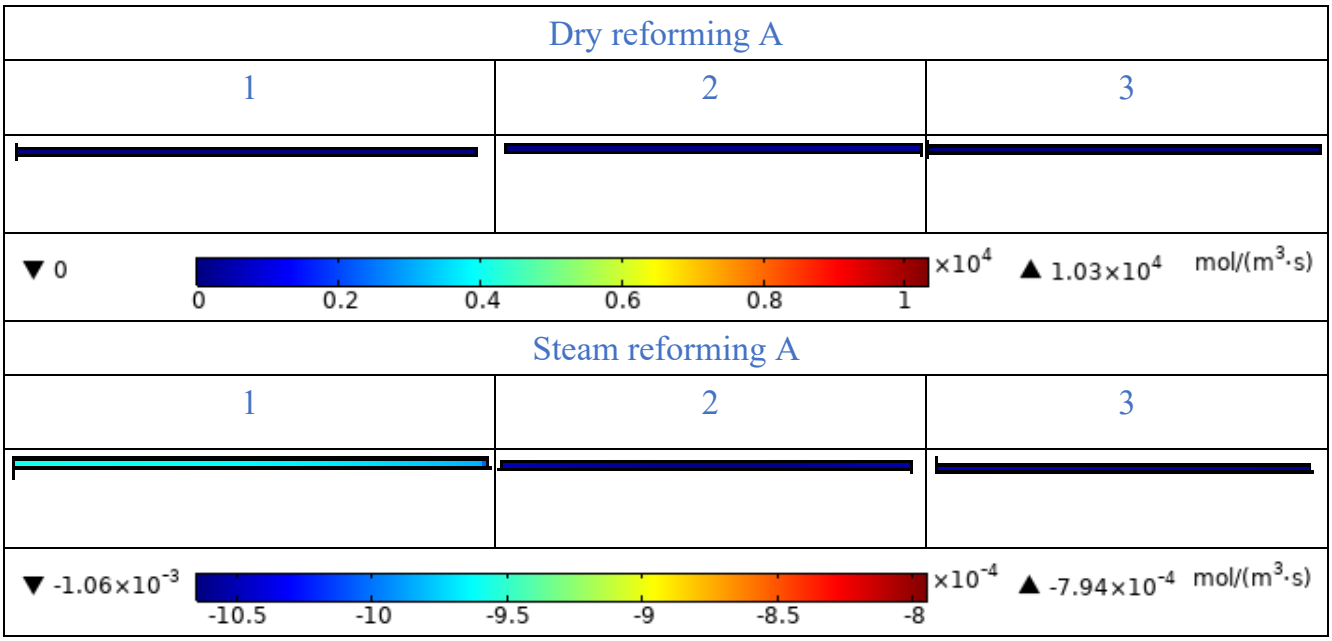

Figure S8. Reaction rate distribution of Steam and dry reforming along the catalyst layers from top to bottom in mol/(m³.s) (A).

F	
Velocity	Partial pressure of water steam
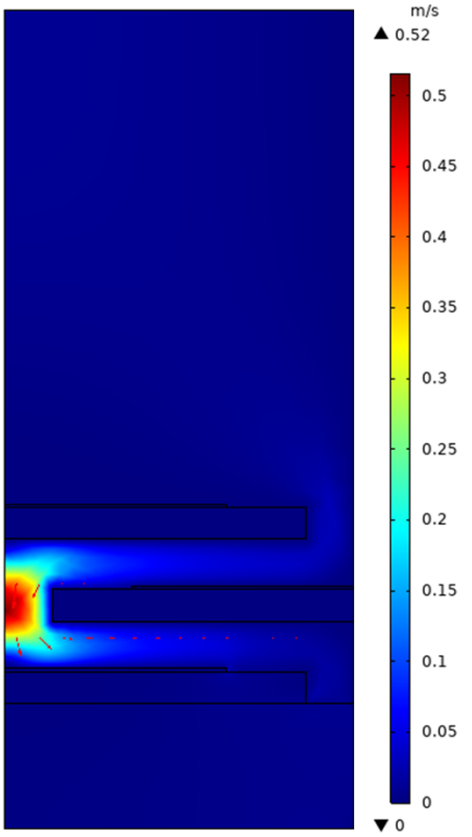	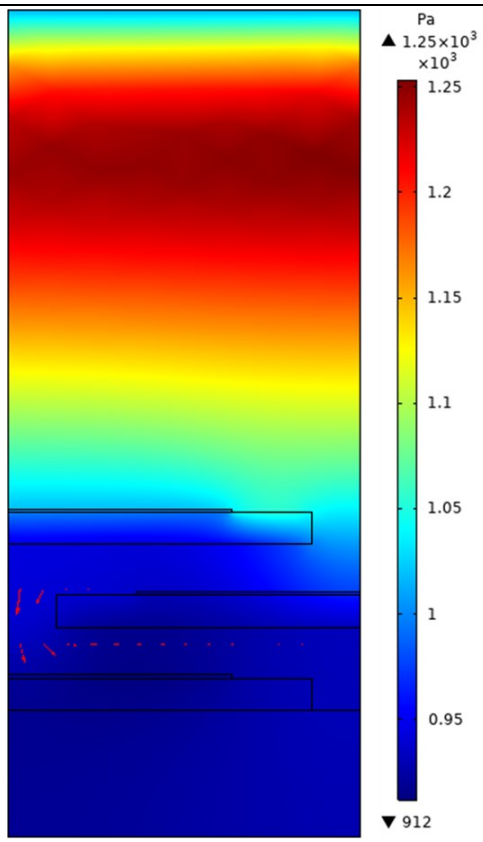

Figure S9. Velocity, partial pressure of steam for F case.

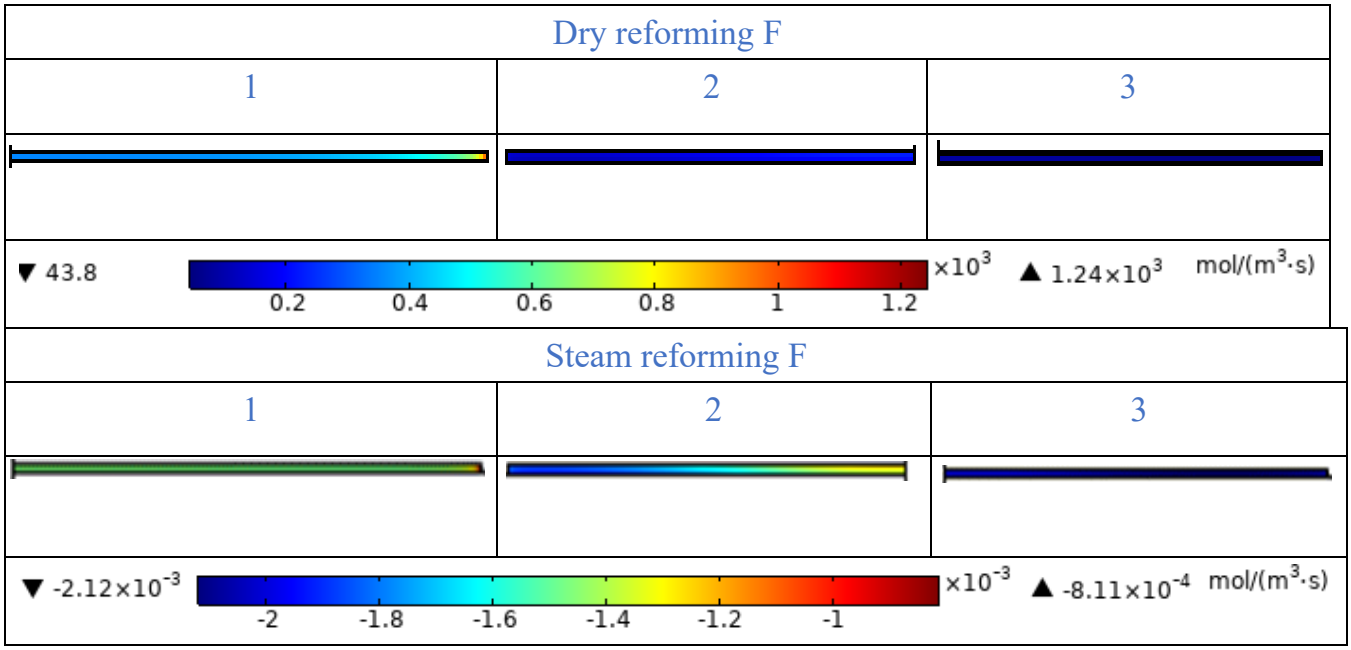

Figure S10. Reaction rate distribution of Steam and dry reforming along the catalyst layers from top to bottom in mol/(m³.s) (F).

G	
Velocity	Partial pressure of water steam
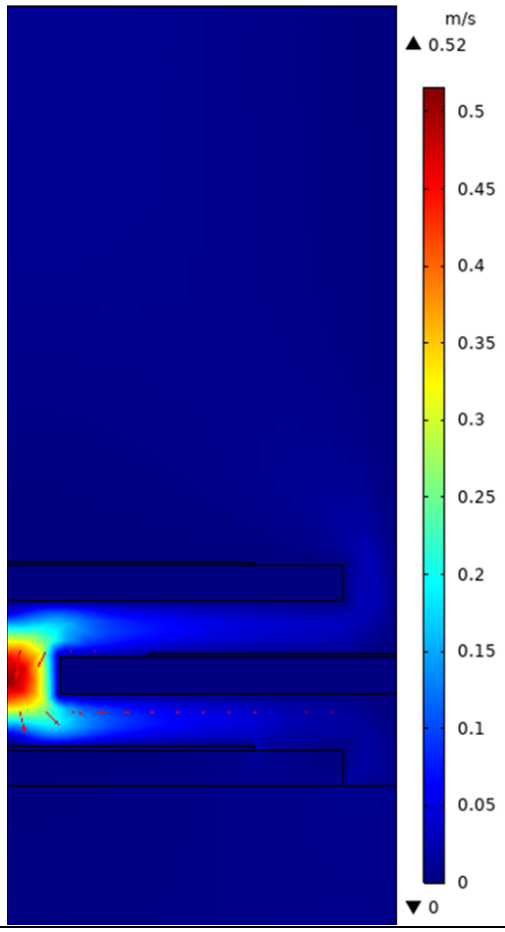	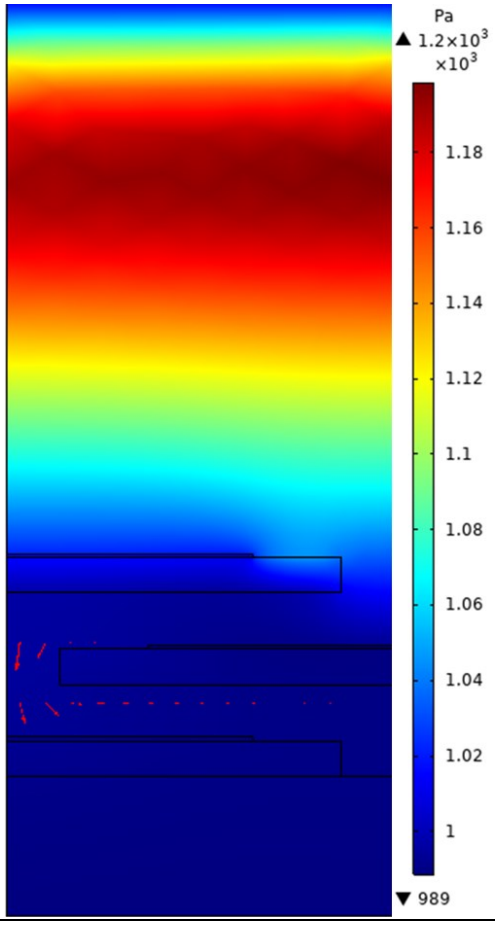

Figure S11. Velocity, partial pressure of steam for G case.

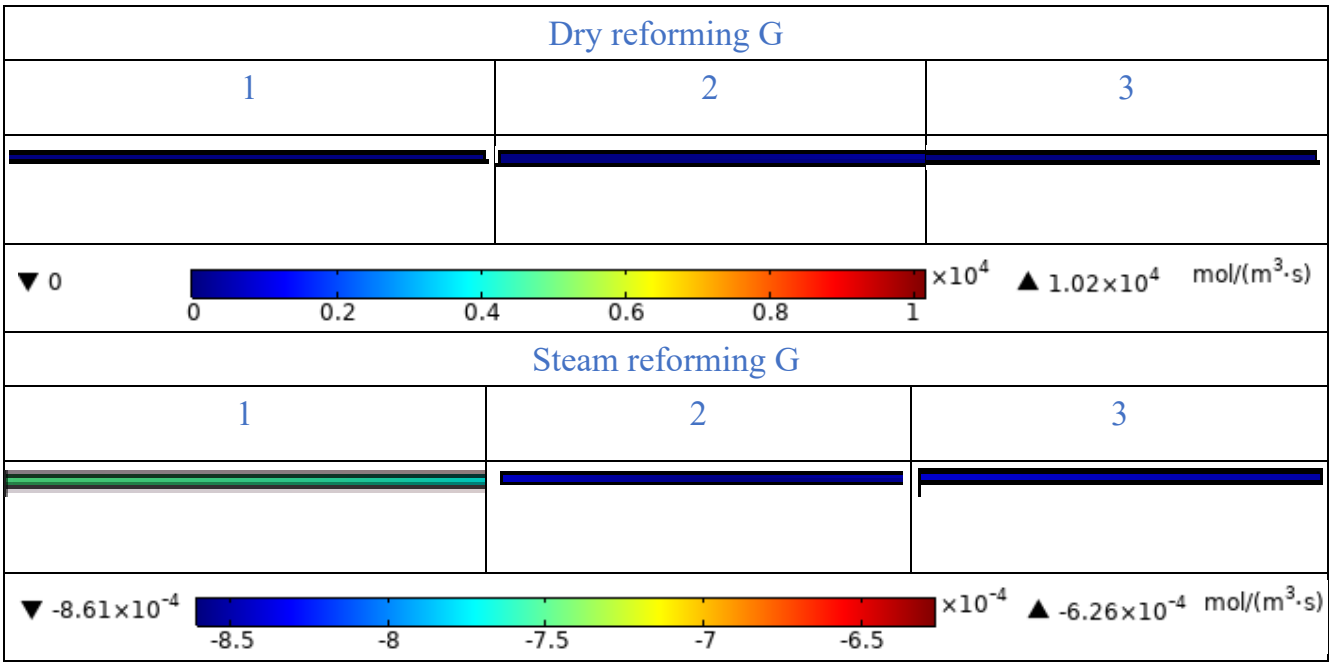

Figure 12. Reaction rate distribution of Steam adnd dry reforming along the catalyst layers from top to bottom in mol/(m³.s) (G).

Reference

18. Lehnert, W.; Meusinger, J.; Thom, F. Modelling of gas transport phenomena in SOFC anodes. *J. Power Sources* **2000**, *87*, 57–63, https://doi.org/10.1016/s0378-7753(99)00356-0.
19. Richardson, J.; Paripatyadar, S. Carbon dioxide reforming of methane with supported rhodium. *Appl. Catal.* **1990**, *61*, 293–309, https://doi.org/10.1016/s0166-9834(00)82152-1.
20. Laurencin, J.; Kane, D.; Delette, G.; Deseure, J.; Lefebvre-Joud, F. Modelling of solid oxide steam electrolyser: Impact of the operating conditions on hydrogen production. *J. Power Sources* **2011**, *196*, 2080–2093, https://doi.org/10.1016/j.jpowsour.2010.09.054.
21. Klein, J.-M.; Georges, S.; Bultel, Y. Modeling of a SOFC Fueled by Methane:Anode Barrier to Allow Gradual Internal Reforming Without Coking. *J. Electrochem. Soc.* **2008**, *155*, B333–B339, https://doi.org/10.1149/1.2838139.
22. Bird ,R. B., Stewart, W. E., Lightfoot, E. N., Transport phenomena, *New York: Wiley*, **2007,** *Revised ed. 2nd, 1-928*, https://isbndb.com/book/9780470115398
23. Reid, R. C., Prausnitz, J. M., Poling, B. E., The properties of gases and liquids, *New York: McGraw-Hill*, **1989**, 4, 9.1-11.43, https://www.osti.gov/biblio/6504847
24. Fuller, E.N.; Schettler, P.D.; Giddings, J.C., New method for prediction of binary gas phase diffusion coefficients, *Ind. Eng. Chem.* **1966**, *58*, 18–27, https://doi.org/10.1021/ie50677a007
25. LE NEINDRE, B., Mesure de la conductivité thermique des liquides et des gaz, *Techniques de l'ingénieur Mesure des grandeurs thermophysiques*, **1996**, RC3, R2920.1-R2920, https://doi.org/10.51257/a-v2-r2920